THE JOURNAL OF PHYSICAL CHEMISTRY C
A JOURNAL OF THE AMERICAN CHEMICAL SOCIETY

pubs.acs.org/JPCC

Article

Crystal Structure Evolution of Fluorine under High Pressure

Christian Tantardini,* Faridun N. Jalolov, and Alexander G. Kvashnin*

Cite This: J. Phys. Chem. C 2022, 126, 11358−11364

Read Online

ACCESS | Metrics & More | Article Recommendations | Supporting Information

ABSTRACT: Fluorinated compounds in the last decade were applied as photo-thermo-refractive glasses, high-stress lubricants, and pharmaceutical drugs due to their good mechanical properties and biocompatibility. Although fluorinated materials are largely employed, the possibility of predicting new structures was limited by the impossibility to use density functional theory (DFT) to describe interatomic and intermolecular interactions correctly. This is seen linearly to increase with fluorine concentration. In crystal structure prediction, modern algorithms are usually combined with first-principles methods employed for global solution, which sometimes fail to describe systems as in the case of strongly correlated materials. Fluorine is one of the tricky elements, which is characterized by relativistic effects and no overlap between the DFT exchange hole and the exact exchange hole. Thus, no relativistic exchange−correlation functional was seen to adequately describe fluorine. In this work, we have found an excellent compromise to investigate fluorinated materials using a combination of SCAN (exchange) and rVV10 (correlation) functionals. This was found through the fundamental study of α- and β-fluorine phases, showing α-fluorine as the most stable structure at temperatures lower than 35 K and 0 GPa with respect to β-fluorine. Further, we have computed crystal structure evolution under pressure looking for new stable fluorine allotropes using the USPEX evolutionary algorithm coupled with the SCAN-rVV10 exchange−correlation functional discovering two phase transitions: one from $C2/c$ (i.e., α-fluorine) to $Cmca$ at ∼5.5 GPa and from $Cmca$ to the $P\bar{4}2_1c$ phase at 220 GPa; all these structures possess metallic behavior. The achievements of this work lie far beyond the thermodynamic of fluorine crystals under pressure. It will give the right instrument to understand the chemical behavior of fluorinated materials under pressure with consequent great speed up to the crystal structure prediction of fluorinated and fluorine-based materials.

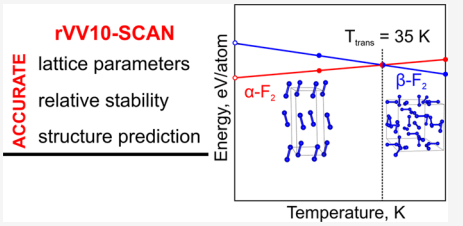

INTRODUCTION

Fluorine is mostly seen as a key element of the 21st century being combined with other elements to generate a class of fluorinated materials employed in several ways. This is because fluorine is the most reactive and lightest element of the halogen group. Due to the high reactivity of fluorine and its position in the Mendeleev periodic table, it is considered as a reference point for the determination of relative electronegativity by Tantardini and Oganov[1] and previously by Pauling[2] in thermochemical scales of electronegativity.

Despite the fact that fluorine is an electron-withdrawing fragment that can be easily incorporated into materials due to its small size and high reactivity, the difficulty in handling fluorine and its toxic properties limited the progress in the chemistry of fluorine. It is noteworthy that fluorine was extracted by electrolyzing a solution of potassium hydrogen fluoride into hydrogen fluoride in 1886 by French chemist Henri Moissan[3,4] who was awarded the Nobel Prize in Chemistry for such a discovery in 1906.

Fluorine showed curious laboratory behavior when it interacts with uranium in uranium hexafluoride to separate the uranium isotopes that allowed fluorine to be subsequently combined with organic compounds exponentially growing up its use.[5−7] Three of the most important fluorinated materials are (i) photo-thermo-refractive (PTR) glasses, (ii) polytetrafluoroethylene (PTFE), and (iii) pharmaceutical drugs. PTR glasses are (oxy)fluorinated glass-ceramics that are composed of nanocrystals of fluorinated rare earth metals embedded in the oxygenated vitreous matrix.[8−10] They are used to produce a broad variety of optical devices, including extra narrow-band filters, wavelength division multiplexing devices, etc.,[11−13] where the photoluminescence of nanoparticles of rare earth is increased by the presence of fluorine.[11−13]

PTFE, commercially known as Teflon AF, is an attractive material not only for automotive but also for bioindustry.[14] Expanded PTFE provides fabric-like properties with controlled pores and high surface area to alter device-related mechanics, processing, and tissue responses while promoting rapid blood clotting. Solid fluoropolymers are also attractive for precise engineering and device processing properties essential to produce several classes of medical devices where fine dimensional tolerances and biocompatibility are required.

Received: March 31, 2022
Revised: June 21, 2022
Published: July 1, 2022

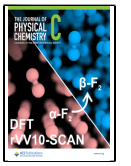

Table 1. Crystal Structure of Bulk α-F_2 Calculated by Using Different Functionals and Different Optimized Norm-Conserving Vanderbilt Pseudopotentials,[35] Norm-Conserving Troullier−Martins,[36] and Gauge Included Plane Augmented Wave (GIPAW)[37] in Comparison with Experimental Data[a]

	lattice parameters				
functional	a, Å	b, Å	c, Å	β, °	volume per cell, Å^3
BP − TM-NC	5.462	3.256	7.185	101.94	125.07
PBE − GIPAW	5.611	3.341	7.423	101.97	136.15
PBE − TM-NC	5.432	3.237	7.122	101.90	122.55
PBE − ONCVP	5.846	3.511	7.075	99.82	143.13
PBESOL − TM-NC	5.395	3.211	6.984	101.62	118.51
PW91 − TM-NC	5.437	3.236	7.158	101.95	123.26
PZ − TM-NC	4.819	3.045	6.029	89.08	88.48
REVPBE − TM-NC	5.512	3.291	7.331	101.96	130.14
SCAN − GIPAW	5.513	3.371	7.129	103.53	128.87
SCAN − TM-NC	5.216	3.239	6.542	98.96	109.21
SCAN − ONCV	5.945	3.548	7.878	102.08	162.53
WC − TM-NC	5.443	3.243	7.146	101.88	123.48
SCAN-RVV10 − GIPAW	**5.494**	**3.364**	**7.113**	**103.41**	**127.91**
PBE from ref 50	5.400	3.265	9.478	133.54	124.58
experiment[51]	5.478	3.270	7.265	102.08	127.13

[a]The SCAN-RVV10 functional with the GIPAW pseudopotential is in bold, which was chosen for further calculations.

This enables the fabrication of multilumen, high-tolerance, small dimensional tubing for advanced catheters.[15]

In the last few decades, fluorinated pharmaceutical drugs were developed and represent ∼20% of all pharmaceutical compounds.[11,16] Worthy to be mentioned are antidepressant fluoxetine (Prozac),[17] the cholesterol-lowering drug atorvastatin (Lipitor),[18] and the antibacterial ciprofloxacin (Ciprobay).[19]

Despite the widespread use of fluorinated compounds, researchers are still not able to explain the behavior of either pure fluorine or fluorine-based compounds leading to modulation of their chemical and mechanical properties.[11,20,21] The deficiency in theoretical studies of fluorine is caused by its unexpected relativistic effects that largely dominate over electron correlation[22] and are very well known for heavier halogen iodine.[23] The Breit-Pauli approximation was seen to describe adequately the relevant atomic levels and the hyperfine structure of fluorine.[22] In this approximation, radial orbitals are frozen from nonrelativistic calculations, while relativistic effects are captured only through the L-S term mixing for a J-value.[22] The necessity of using a Dirac Hamiltonian to solve the relativistic Schrödinger equation made it impossible to successfully use heuristic density functional theory (DFT) to study solid fluorine at both zero and high pressures.

In this work, we would like to correctly describe the structure of solid fluorine as a function of pressure and temperature using a nonrelativistic Hamiltonian in the framework of DFT. This idea came to us from a previous study by Mattsson et al.[24] where the post-Hartree−Fock approach without a relativistic Hamiltonian was seen to describe the loss of σ-hole interaction in the fluorine alpha phase, which makes the $C2/c$ phase of fluorine (α-phase) more stable with respect to the $Cmca$ phase. Thus, the symmetry of α-fluorine ($C2/c$) differs from the symmetry of the heavy halogen α-phase ($Cmca$).[24]

Here, we found that the rVV10[25] correlation DFT functional in combination with exchange DFT functional meta-GGA of Perdew−Burke−Ernzerhof, so called SCAN,[26] is the best choice for DFT without a relativistic Hamiltonian to describe the structure of bulk fluorine. This approach (SCAN-rVV10) was subsequently used for crystal structure prediction of bulk fluorine at pressures from 0 to 300 GPa combined with the evolutionary algorithm USPEX. Predicted phases at 0 GPa were carefully studied, and temperature dependence of the stability of the α- and β-F_2 phases was defined showing that a major contribution to the stability of the β-F_2 phase comes from configurational entropy.

COMPUTATIONAL DETAILS

α-Fluorine structure from the neutron diffraction experiment was used to validate several combinations of DFT functionals and pseudopotentials. The criterion for correctness of the chosen approach was to obtain results comparable to the experiment with an error below 2%.[27] We used different combinations of Perdew−Burke−Ernzerhof (PBE),[28] PBEsol,[29] Perdew−Zunger (PZ),[30] Perdew−Wang (PW91),[31] Becke−Perdew (BP),[32,33] WC,[34] SCAN,[26] and rVV10[25] functionals together with norm-conserving pseudopotentials: optimized norm-conserving Vanderbilt pseudopotential,[35] norm-conserving Troullier−Martins,[36] and gauge included plane augmented wave (GIPAW).[37]

Prediction of crystal structures of solid fluorine at a pressure range from 0 to 300 GPa was performed by using the fixed-composition evolutionary algorithm USPEX,[38−40] which was interfaced with the Quantum Espresso package[41,42] to relax crystal structures during the search. If the found structures are optimized without constrains, the space group is assigned considering the tolerance on the atomic positions (reduced coordinates), primitive vectors, equal to 10^{-4}. The first generation of 120 structures was generated using random symmetric[40] and random topological generators.[43] The succeeding generations were obtained by applying the heredity (40% of each generation), soft-mutation (20%), and transmutation (20%) operators; 20% of each generation was produced using random symmetric and random topological generators. The structure relaxations and total energy computations were performed using Quantum ESPRESSO. The meta-GGA SCAN[26] with GIPAW was used for the exchange−correlation functional in combination with the

https://doi.org/10.1021/acs.jpcc.2c02213
J. Phys. Chem. C 2022, 126, 11358−11364

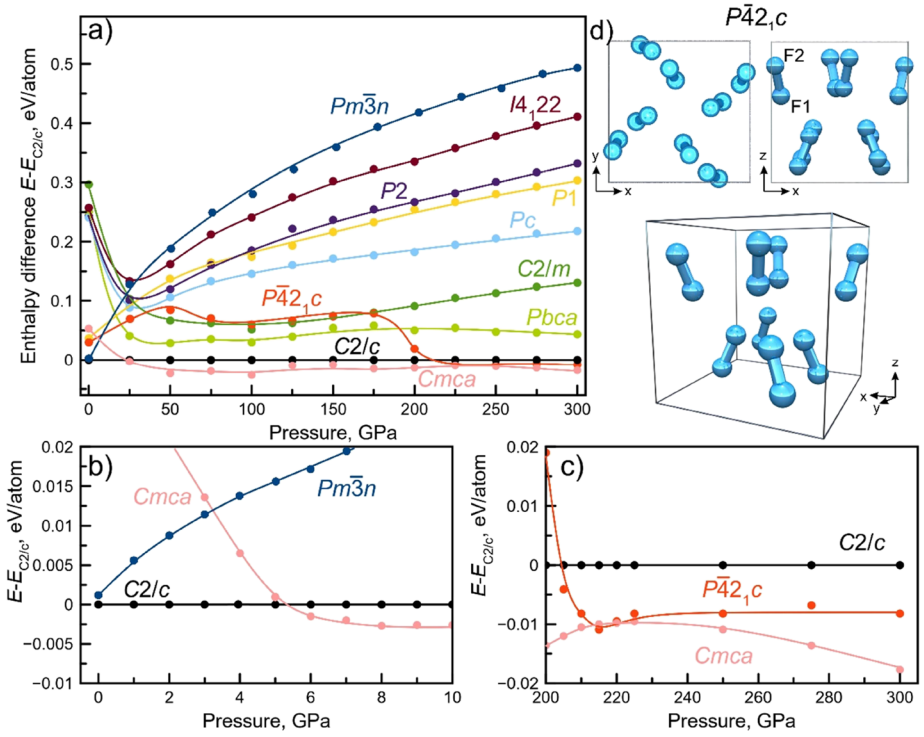

Figure 1. Dependencies of the enthalpy difference ($E - E_{C2/c}$) on the pressure for pressure ranges (a) 0−300 GPa, (b) 0−10 GPa to show transition from α-F_2 to the *Cmca* phase and (c) 200−300 GPa; (d) top, side, and isometric views of the crystal structure of $P\bar{4}2_1c$ fluorine. Solid lines are a guide to the eye.

rVV10 DFT functional[25] for vdW correction. A plane-wave energy cutoff of 90 Ry and a Gaussian smearing of electronic occupations of 0.005 eV together with a generated Γ-centered k-point grid with the length of the smallest vector in k-space equal to 0.025 $Å^{-1}$ ensured the convergence of total energies equal to 10^{-5} Ry and forces cutoff equal to 10^{-6} Ry.

The temperature stability of α- and β-F_2 allotropes at 0 GPa was studied by using Born-Oppenheimer ab initio molecular dynamics (BOMD) that was performed with the same SCAN-rVV10 DFT functional. This was done because it was not possible to calculate phonon spectra with density functional perturbational theory (DFPT) using the SCAN-rVV10 DFT functional due to the different formalism of algorithms of SCAN (meta-GGA)[44−46] and rVV10.[47] The efficiency of BOMD to determinate the temperature stability was confirmed by results obtained in the "Results and Discussion" Section that agreed with experimental results of α- and β-F_2 allotropes. We performed BOMD simulations at temperatures 20 and 50 K executing 5000 steps with a timestep of 20 a.u. (~1 fs). The relaxation of the system was performed according to the Beeman dynamics with the damped Beeman algorithm for the ionic dynamics[48] and the Parrinello−Rahman-extended Lagrangian for the cell dynamics.[49]

Evolution of Helmholtz free energy with time allowed us to calculate the average energy at finite temperatures (20 and 50 K). These data were extrapolated to 0 K to determine the ground state energy of α- and β-F_2 allotropes at 0 K, which contains zero-point energy (ZPE) contribution. Thus, ZPE of both phases was calculated from the difference between DFT and extrapolated BOMD energies at 0 K.

RESULTS AND DISCUSSION

Optimal DFT Approach for Calculation. To define the optimal DFT functional, we have tested all DFT functionals known up-to-date to relax the crystal structure of the α-F_2 phase coming from neutron diffraction,[24] and SCAN-rVV10 showed symmetry preservation ($C2/c$) with the difference in volume compared to the experiment of about 0.5%. Data about the calculated crystal structure of α-fluorine are presented in Table 1. This can be considered as an accurate result being a common acceptable error due to DFT in the order of 2%. All other DFT functionals and SCAN without rVV10 increased the volume by more than 2%, and most importantly, they did not preserve the symmetry. As we know, the mean radii of Dirac−Hartree−Fock and Hartree−Fock (HF) orbitals, $\langle r\rangle_{1s}^{DHF}$ = 0.17543 and $\langle r\rangle_{1s}^{HF}$ = 0.17567 bohr, and a difference of 0.14% are corrected by Breit-Pauli approximation.[22] This relativistic contraction in fluorine seems to make its exact exchange hole close to its electron, and it can be actually described by the SCAN exchange functional because it contains a local term (i.e., electronic localization function), which allows the overlap between the DFT exchange hole and the exact exchange hole.[26]

If the exchange term is correctly reproduced by SCAN, the correlation term needs a different functional to measure how much the movement of each electron is influenced by the presence of all other electrons. This issue is efficiently solved by the rVV10 functional that is a gradient-generalized DFT functional with a nonlocal correlation term.[25] Such a DFT functional was explicitly developed to include the dispersion interactions that originate from correlations between charge fluctuations in different parts of an extended system, which can be taken into account via the full frequency-dependent electronic polarizability in the formally adiabatic-coupling

https://doi.org/10.1021/acs.jpcc.2c02213
J. Phys. Chem. C 2022, 126, 11358−11364

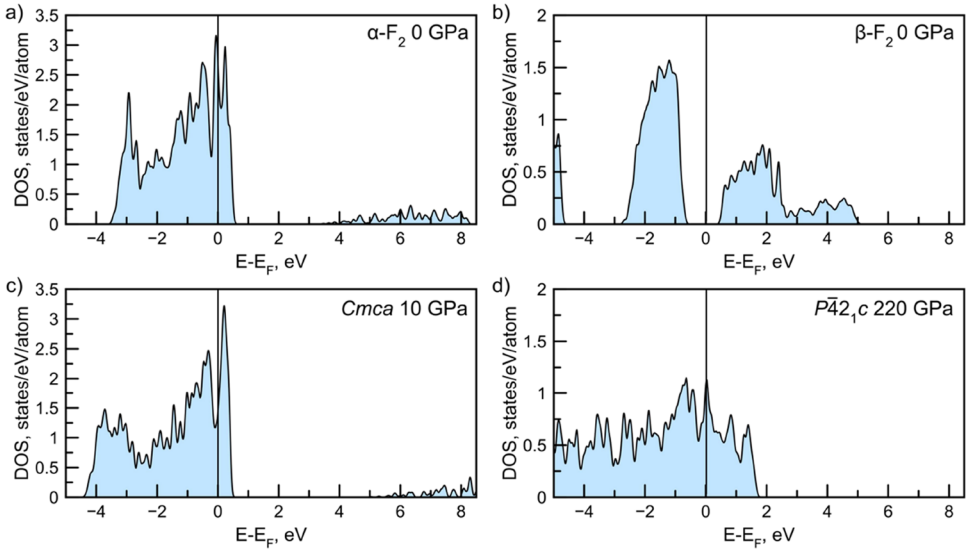

Figure 2. Calculated electronic density of states for (a) α-F_2 ($C2/c$), (b) β-F_2 ($Pm\bar{3}n$) at 0 GPa, and (c) $Cmca$ at 10 GPa, and (d) $P\bar{4}2_1c$ and 220 GPa. Fermi energy is shifted to zero.

fluctuation-dissipation formalism.[52,53] Furthermore, the combination of SCAN with rVV10 is documented to fit vdW interactions very well that are present in fluorine structure.[54]

It is worth noting that a feasible approach to treat long-range dispersions allows the right understanding of vdW interactions that rule the chemical bonding within the crystal structure and that they can fully described by topological study.[55−58]

High-Pressure Stability. The achieved success of SCAN-rVV10 allowed us to subsequently study the crystal structure of bulk fluorine under pressure within a range between 0 and 300 GPa. During the searches at different pressures, nine structures were chosen for further consideration having various space groups, namely, $I4_122$, $Cmca$, $Pbca$, $P\bar{4}2_1c$, $C2/m$, $C2/c$ (α-fluorine), Pc, $P1$, and $P2$. We have also added and considered the β-phase in the high-pressure search. This phase of fluorine is experimentally known to be characterized by disordered crystal structure with a $Pm\bar{3}n$ space group.[55] Crystal data of considered structures are presented in Table S1, Supporting Information. Several local structures of β-fluorine were constructed based on the average disordered structure from an experiment by Jordan et al.[59] We found that all the calculated β-fluorine approximants have similar energies. Thus, for further calculations of the β-phase, we have considered only one local structure.

Dependencies of enthalpies on the pressure for predicted fluorine structures are shown in Figure 1. One can note that β-fluorine is ∼1.5 meV/atom higher in energy than α-fluorine at 0 K and 0 GPa (zero-point energy contribution was not taken into account). Such a small energy difference may be overcome by insufficient entropy contribution. Moreover, as the pressure increases, α-fluorine remains the most thermodynamically stable phase from 0 to 5 GPa (see Figure 1a,b). A previous study[24] showed that the $Cmca$ phase is more stable than $C2/c$ for halogens except for fluorine. This is due to the lack of significantly stabilizing σ-hole interactions in fluorine that makes the $C2/c$ phase more energetically favorable with respect to the $Cmca$ counterpart in a vacuum. As we increase the pressure, the proximity between the F_2 molecules at ∼5.5 GPa allows the formation of σ-hole interactions and $Cmca$ becomes more thermodynamically stable with respect to $C2/c$ (see Figure 1a,b). At higher pressures, the only dominant phase is the $Cmca$ until the pressure exceeds 220 GPa, where the transition to the tetragonal $P\bar{4}2_1c$ phase was observed (see Figure 1c). The crystal structure of the $P\bar{4}2_1c$ phase, shown in Figure 1d, contains two symmetrically inequivalent fluorine atoms both occupying two 8e Wyckoff positions. The detailed information about crystal data of the $P\bar{4}2_1c$ phase is presented in Table S1 (Supporting Information). All other predicted phases are metastable (have a higher enthalpy compared to α-fluorine). In the pressure range 50−100 GPa, the second lowest-energy structure has a $Pbca$ space group with the enthalpy difference with $C2/c$ structure of ∼0.05 eV/atom (see Figure 1a). We would like to note that our results contradict recent data obtained by Lv et al.,[50] which were performed with a PBE DFT functional that, as we explained at the beginning of our study, is not the right choice in the case of the fluorine system.

Albeit α- and β-phases are molecular crystals, we can see that at 0 GPa they have a different electronic behavior. We showed that α-F_2 behaves as a metal, i.e., nonzero density of state at the Fermi level (E_F = 6.975 eV) and β-F_2 is a semiconductor with a band gap equal to 0.834 eV (E_F = 11.825 eV) as shown by calculated densities of states (DOS) in Figure 2a,b. The observed phase transition from α-F_2 to $Cmca$ (both are molecular crystals) keeps the metallic behavior unchanged as seen from calculated DOS at 10 GPa for $Cmca$ (see Figure 2c). At 220 GPa, the most stable phase is $P\bar{4}2_1c$, which is a molecular crystal showing metallic behavior (nonzero density of state at the Fermi level of 21.573 eV), see Figure 2d.

Temperature Stability at 0 GPa. Another issue that should be addressed is the temperature stability of α- and β-fluorine at 0 GPa, which can be estimated by calculations of entropy contributions. It is noteworthy that the long-range correction is not available in the formalism of DFPT.[60,61] Thus, the only possibilities were to perform ab initio molecular dynamics at finite temperatures in order to obtain energy changes of each phase with the increasing temperature. As the melting temperature of fluorine equals to 53.48 K,[7] we performed MD simulations at 20 and 50 K for α- and β-fluorine at 0 GPa. Results of simulations are shown in Figure

https://doi.org/10.1021/acs.jpcc.2c02213
J. Phys. Chem. C 2022, 126, 11358−11364

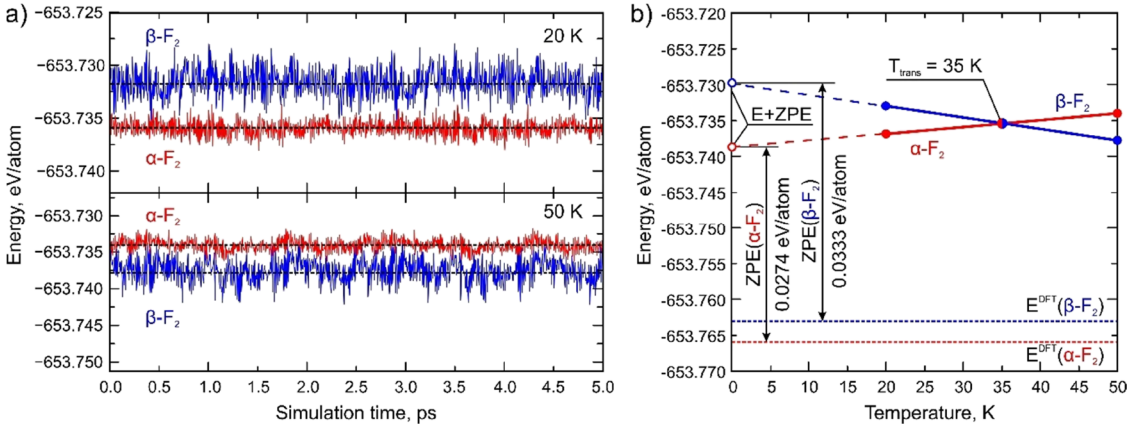

Figure 3. (a) Evolution of Helmholtz free energy with time during Born-Oppenheimer molecular dynamics for α- and β-phases (red and blue colors) at 20 and 50 K. Horizontal dashed lines denote average values; (b) calculated dependence of averaged Helmholtz free energies on temperature. Red and blue horizontal lines represent the total energy of α- and β-fluorine calculated by DFT at 0 K.

3a. One can see that at 20 K, α-fluorine has a lower energy compared to β-fluorine with an energy difference of about 4 meV/atom. Only at a simulated temperature of 50 K, the energy of the β-phase becomes lower than that of the α-phase. The averaged values of energies depending on temperature are shown in Figure 3b. Detailed information is presented in the Supporting Information (see Table S2). The obtained dependence was extrapolated to 0 K to determine the energy that contains ZPE. Thus, the difference between DFT-calculated energy and extrapolated one determines ZPE of each fluorine phase (see Figure 3b). As a result, the zero-point energy of the α-phase is 27.42 eV/atom, while for the β-phase, ZPE = 33.31 eV/atom. The ZPE value for α-F_2 agrees well with reference data for the zero-point energy of the isolated F_2 molecule, which equals to 55.42 eV/F_2 (447 cm^{-1}).[62]

Such a good agreement ensures us correct results in the computation of transition temperature, which was obtained to be ~35 K (see Figure 3b). The obtained transition temperature is lower than that measured in experiments (45.6 K[51]), which can be explained by insufficient length of MD simulation, or MD simulations should be carried out at lower temperatures, which are further from the melting temperature of fluorine.

CONCLUSIONS

This work is the first DFT study where we correctly describe the interatomic and intermolecular interaction of the fluorine crystal with high accuracy by using the SCAN-rVV10 DFT functional. Our study opens the possibility to improve crystal structure prediction of fluorinated and fluorine-based materials. In fact, the combination of SCAN-rVV10 and evolutionary algorithm USPEX was fruitfully used to predict the high-pressure chemistry of fluorine seeing two-phase transition, namely, $C2/c \rightarrow Cmca$ at 5 GPa and $Cmca \rightarrow P\bar{4}2_1c$ at 220 GPa. Electronic structure calculations show the metallization of the *Cmca* phase at high pressures, indicating the formation of atomic crystals instead of molecules as α-F_2. The transition temperature from α- to β-phases was found to be 35 K by using ab initio molecular dynamics with the SCAN-rVV10 DFT functional, which agrees well with experimental results. Thus, our study opens the door for further investigations of fluorinated and fluorine-based materials by using crystal structure prediction algorithms with the proposed DFT functional.

ASSOCIATED CONTENT

Supporting Information

The Supporting Information is available free of charge at https://pubs.acs.org/doi/10.1021/acs.jpcc.2c02213.

Data on crystal structures of predicted compounds and temperature contribution to stability of fluorine phases (PDF)

AUTHOR INFORMATION

Corresponding Authors

Alexander G. Kvashnin − *Skolkovo Institute of Science and Technology, Moscow 121205, Russian Federation;* orcid.org/0000-0002-0718-6691; Email: A.Kvashnin@skoltech.ru

Christian Tantardini − *Hylleraas Center, Department of Chemistry, UiT The Arctic University of Norway, N-9037 Tromsø, Norway; Institute of Solid State Chemistry and Mechanochemistry SB RAS, 630128 Novosibirsk, Russian Federation;* orcid.org/0000-0002-2412-9859; Email: christiantantardini@ymail.com

Author

Faridun N. Jalolov − *Skolkovo Institute of Science and Technology, Moscow 121205, Russian Federation*

Complete contact information is available at: https://pubs.acs.org/10.1021/acs.jpcc.2c02213

Notes

The authors declare no competing financial interest.

ACKNOWLEDGMENTS

The authors would like to thank Prof. Dr. Xavier Gonze of UCLouvain, Dr. Davide Ceresoli of CNR Milano, and Dr. Suman Chowdhury of Indian Institute of Science for useful discussion. Dr. Davide Ceresoli developed the GIPAW pseudopotential of fluorine that we have used in this article. The authors would like to thank the Siberian Super-Computer Center of the Siberian Branch of the Russian Academy of Sciences and Sigma2−the National Infrastructure for High Performance Computing Data Storage in Norway−for computational resources. This work was supported by Russian state assignment to ISSCM SB RAS (project No. FWUS-2021-0005).

REFERENCES

(1) Tantardini, C.; Oganov, A. R. Thermochemical Electronegativities of the Elements. *Nat. Commun.* **2021**, *12*, 2087.
(2) Pauling, L. The Nature of The Chemical Bond. Iv. The Energy of Single Bonds And The Relative Electronegativity of Atoms. *J. Am. Chem. Soc.* **1932**, *54*, 3570−3582.
(3) Moissan, H. Action d'un Courant Électrique Sur l'acide Fluorhydrique Anhydre [The Action of an Electric Current on Anhydrous Hydrofluoric Acid]. *Comptes Rendus Hebd. Séances Académie Sci. Fr.* **1886**, *102*, 1543−1544.
(4) Moissan, H. Sur La Décomposition de l'acide Fluorhydrique Par Un Courant Électrique [On the Decomposition of Hydrofluoric Acid by an Electric Current]. *Comptes Rendus Hebd. Séances Académie Sci.* **1886**, *103*, 202.
(5) Barry, A.; Bergeron, A.; Stoddard, T.; Crigger, B.; Hamilton, H.; Maybee, A. Fluoride Volatility Experiments on Irradiated Thoria Fuel at Canadian Nuclear Laboratories. *J. Fluorine Chem.* **2018**, *214*, 8−12.
(6) Homma, S.; Uoi, Y.; Braun, A.; Koga, J.; Matsumoto, S. Reaction Model for Fluorination of Uranium Dioxide Using Improved Unreacted Shrinking Core Model for Expanding Spherical Particles. *J. Nucl. Sci. Technol.* **2008**, *45*, 823−827.
(7) Haynes, W. M. *CRC Handbook of Chemistry and Physics*; CRC Press, 2014.
(8) Stookey, S. D.; Beall, G. H.; Pierson, J. E. Full-color Photosensitive Glass. *J. Appl. Phys.* **1978**, *49*, 5114−5123.
(9) Pierson, E. J.; Stookey, S. D. Photosensitive Colored Glasses. 4017318.
(10) Pierson, E. J.; Stookey, S. D. Method for Making Photosensitive Colored Glasses. 4057408.
(11) Reichenbächer, K.; Süss, H. I.; Hulliger, J. Fluorine in Crystal Engineering—"the Little Atom That Could.". *Chem. Soc. Rev.* **2005**, *34*, 22−30.
(12) Brandily-Anne, M.-L.; Lumeau, J.; Glebova, L.; Glebov, L. B. Specific Absorption Spectra of Cerium in Multicomponent Silicate Glasses. *J. Non-Cryst. Solids* **2010**, *356*, 2337−2343.
(13) Lumeau, J.; Zanotto, E. D. A Review of the Photo-Thermal Mechanism and Crystallization of Photo-Thermo-Refractive (PTR) Glass. *Int. Mater. Rev.* **2017**, *62*, 348−366.
(14) Biswas, S. K.; Vijayan, K. Friction and Wear of PTFE — a Review. *Wear* **1992**, *158*, 193−211.
(15) Khedkar, J.; Negulescu, I.; Meletis, E. I. Sliding Wear Behavior of PTFE Composites. *Wear* **2002**, *252*, 361−369.
(16) Müller, K.; Faeh, C.; Diederich, F. Fluorine in Pharmaceuticals: Looking Beyond Intuition. *Science* **2007**, *317*, 1881−1886.
(17) Wong, D. T.; Bymaster, F. P.; Engleman, E. A. Prozac (Fluoxetine, Lilly 110140), the First Selective Serotonin Uptake Inhibitor and an Antidepressant Drug: Twenty Years since Its First Publication. *Life Sci.* **1995**, *57*, 411−441.
(18) Roth, B. D. 1 The Discovery and Development of Atorvastatin, A Potent Novel Hypolipidemic Agent. In *Progress in Medicinal Chemistry*; King, F. D., Oxford, A. W., Reitz, A. B., Dax, S. L., Eds.; Elsevier, 2002; Vol. *40*, pp. 1−22.
(19) Karl, D.; Muhammad, M. Fluoroquinolones: Action and Resistance. *Curr. Top. Med. Chem.* **2002**, *3*, 249−282.
(20) Pagliaro, M.; Ciriminna, R. New Fluorinated Functional Materials. *J. Mater. Chem.* **2005**, *15*, 4981−4991.
(21) Liu, Y.; Jiang, L.; Wang, H.; Wang, H.; Jiao, W.; Chen, G.; Zhang, P.; Hui, D.; Jian, X. A Brief Review for Fluorinated Carbon: Synthesis, Properties and Applications. *Nanotechnol. Rev.* **2019**, *8*, 573−586.
(22) Boualili, F. Z.; Nemouchi, M.; Godefroid, M.; Jönsson, P. Weak Correlation and Strong Relativistic Effects on the Hyperfine Interaction in Fluorine. *ArXiv210801116 Phys.* 2021.
(23) Tantardini, C.; Michalchuk, A. A. L. Dess-Martin Periodinane: The Reactivity of a Λ5-Iodane Catalyst Explained by Topological Analysis. *Int. J. Quantum Chem.* **2019**, *119*, No. e25838.
(24) Mattsson, S.; Paulus, B.; Redeker, F. A.; Beckers, H.; Riedel, S.; Müller, C. The Crystal Structure of α-F2: Solving a 50 Year Old Puzzle Computationally. *Chem. − Eur. J.* **2019**, *25*, 3318−3324.
(25) Vydrov, O. A.; Van Voorhis, T. Nonlocal van Der Waals Density Functional: The Simpler the Better. *J. Chem. Phys.* **2010**, *133*, No. 244103.
(26) Yao, Y.; Kanai, Y. Plane-Wave Pseudopotential Implementation and Performance of SCAN Meta-GGA Exchange-Correlation Functional for Extended Systems. *J. Chem. Phys.* **2017**, *146*, 224105.
(27) Sim, E.; Song, S.; Burke, K. Quantifying Density Errors in DFT. *J. Phys. Chem. Lett.* **2018**, *9*, 6385−6392.
(28) Perdew, J. P.; Burke, K.; Ernzerhof, M. Generalized Gradient Approximation Made Simple [Phys. Rev. Lett. 77, 3865 (1996)]. *Phys. Rev. Lett.* **1997**, *78*, 1396−1396.
(29) Perdew, J. P.; Ruzsinszky, A.; Csonka, G. I.; Vydrov, O. A.; Scuseria, G. E.; Constantin, L. A.; Zhou, X.; Burke, K. Restoring the Density-Gradient Expansion for Exchange in Solids and Surfaces. *Phys. Rev. Lett.* **2008**, *100*, No. 136406.
(30) Perdew, J. P.; Zunger, A. Self-Interaction Correction to Density-Functional Approximations for Many-Electron Systems. *Phys. Rev. B* **1981**, *23*, 5048.
(31) Wang, Y.; Perdew, J. P. Correlation Hole of the Spin-Polarized Electron Gas, with Exact Small-Wave-Vector and High-Density Scaling. *Phys. Rev. B* **1991**, *44*, 13298−13307.
(32) Perdew, J. P. Density-Functional Approximation for the Correlation Energy of the Inhomogeneous Electron Gas. *Phys. Rev. B* **1986**, *33*, 8822.
(33) Becke, A. D. Density-Functional Exchange-Energy Approximation with Correct Asymptotic Behavior. *Phys. Rev. A* **1988**, *38*, 3098−3100.
(34) Wu, Z.; Cohen, R. E. More Accurate Generalized Gradient Approximation for Solids. *Phys. Rev. B* **2006**, *73*, No. 235116.
(35) Hamann, D. R. Optimized Norm-Conserving Vanderbilt Pseudopotentials. *Phys. Rev. B* **2013**, *88*, No. 085117.
(36) Troullier, N.; Martins, J. L. Efficient Pseudopotentials for Plane-Wave Calculations. *Phys. Rev. B* **1991**, *43*, 1993−2006.
(37) Pickard, C. J.; Mauri, F. All-Electron Magnetic Response with Pseudopotentials: NMR Chemical Shifts. *Phys. Rev. B* **2001**, *63*, No. 245101.
(38) Oganov, A. R.; Glass, C. W. Crystal Structure Prediction Using Ab Initio Evolutionary Techniques: Principles and Applications. *J. Chem. Phys.* **2006**, *124*, 244704.
(39) Oganov, A. R.; Lyakhov, A. O.; Valle, M. How Evolutionary Crystal Structure Prediction Works—and Why. *Acc. Chem. Res.* **2011**, *44*, 227−237.
(40) Lyakhov, A. O.; Oganov, A. R.; Stokes, H. T.; Zhu, Q. New Developments in Evolutionary Structure Prediction Algorithm USPEX. *Comput. Phys. Commun.* **2013**, *184*, 1172−1182.
(41) Giannozzi, P.; Baroni, S.; Bonini, N.; Calandra, M.; Car, R.; Cavazzoni, C.; Ceresoli, D.; Chiarotti, G. L.; Cococcioni, M.; Dabo, I.; Dal Corso, A.; de Gironcoli, S.; Fabris, S.; Fratesi, G.; Gebauer, R.; Gerstmann, U.; Gougoussis, C.; Kokalj, A.; Lazzeri, M.; Martin-Samos, L.; Marzari, N.; Mauri, F.; Mazzarello, R.; Paolini, S.; Pasquarello, A.; Paulatto, L.; Sbraccia, C.; Scandolo, S.; Sclauzero, G.; Seitsonen, A. P.; Smogunov, A.; Umari, P.; Wentzcovitch, R. M. QUANTUM ESPRESSO: A Modular and Open-Source Software Project for Quantum Simulations of Materials. *J. Phys. Condens. Matter* **2009**, *21*, No. 395502.
(42) Giannozzi, P.; Andreussi, O.; Brumme, T.; Bunau, O.; Nardelli, M. B.; Calandra, M.; Car, R.; Cavazzoni, C.; Ceresoli, D.; Cococcioni, M.; et al. Advanced Capabilities for Materials Modelling with Quantum ESPRESSO. *J. Phys. Condens. Matter* **2017**, *29*, 465901.
(43) Bushlanov, P. V.; Blatov, V. A.; Oganov, A. R. Topology-Based Crystal Structure Generator. *Comput. Phys. Commun.* **2019**, *236*, 1−7.
(44) Baroni, S.; de Gironcoli, S.; Dal Corso, A.; Giannozzi, P. Phonons and Related Crystal Properties from Density-Functional Perturbation Theory. *Rev. Mod. Phys.* **2001**, *73*, 515−562.
(45) Giannozzi, P.; Baroni, S. Density-Functional Perturbation Theory. In *Handbook of Materials Modeling: Methods*; Yip, S., Ed.; Springer Netherlands: Dordrecht, 2005; pp. 195−214.

https://doi.org/10.1021/acs.jpcc.2c02213
J. Phys. Chem. C 2022, 126, 11358−11364

(46) Baroni, S.; Giannozzi, P.; Isaev, E. Density-Functional Perturbation Theory for Quasi-Harmonic Calculations. *Rev. Mineral. Geochem.* **2010**, *71*, 39−57.
(47) Sabatini, R.; Küçükbenli, E.; Pham, C. H.; de Gironcoli, S. Phonons in Nonlocal van Der Waals Density Functional Theory. *Phys. Rev. B* **2016**, *93*, No. 235120.
(48) Beeman, D. Some Multistep Methods for Use in Molecular Dynamics Calculations. *J. Comput. Phys.* **1976**, *20*, 130−139.
(49) Parrinello, M.; Rahman, A. Crystal Structure and Pair Potentials: A Molecular-Dynamics Study. *Phys. Rev. Lett.* **1980**, *45*, 1196−1199.
(50) Lv, Q.; Jin, X.; Cui, T.; Zhuang, Q.; Li, Y.; Wang, Y.; Bao, K.; Meng, X. Crystal Structures and Electronic Properties of Solid Fluorine under High Pressure. *Chin. Phys. B* **2017**, *26*, No. 076103.
(51) Ivlev, S. I.; Karttunen, A. J.; Hoelzel, M.; Conrad, M.; Kraus, F. The Crystal Structures of α- and β-F2 Revisited. *Chem. − Eur. J.* **2019**, *25*, 3310−3317.
(52) Langreth, D. C.; Perdew, J. P. The Gradient Approximation to the Exchange-Correlation Energy Functional: A Generalization That Works. *Solid State Commun.* **1979**, *31*, 567−571.
(53) Langreth, D. C.; Perdew, J. P. Exchange-Correlation Energy of a Metallic Surface: Wave-Vector Analysis. *Phys. Rev. B* **1977**, *15*, 2884−2901.
(54) Peng, H.; Yang, Z.-H.; Perdew, J. P.; Sun, J. Versatile van Der Waals Density Functional Based on a Meta-Generalized Gradient Approximation. *Phys. Rev. X* **2016**, *6*, No. 041005.
(55) Tantardini, C.; Ceresoli, D.; Benassi, E. Source Function and Plane Waves: Toward Complete Bader Analysis. *J. Comput. Chem.* **2016**, *37*, 2133−2139.
(56) Fedorov, A. Y.; Drebushchak, T. N.; Tantardini, C. Seeking the Best Model for Non-Covalent Interactions within the Crystal Structure of Meloxicam. *Comput. Theor. Chem.* **2019**, *1157*, 47−53.
(57) Tantardini, C.; Michalchuk, A. A. L.; Samtsevich, A.; Rota, C.; Kvashnin, A. G. The Volumetric Source Function: Looking Inside van Der Waals Interactions. *Sci. Rep.* **2020**, *10*, 7816.
(58) Arkhipov, S. G.; Sherin, P. S.; Kiryutin, A. S.; Lazarenko, V. A.; Tantardini, C. The Role of S-Bond in Tenoxicam Keto−Enolic Tautomerization. *CrystEngComm* **2019**, *21*, 5392−5401.
(59) Jordan, T. H.; Streib, W. E.; Lipscomb, W. N. Single-Crystal X-Ray Diffraction Study of B-Fluorine. *J. Chem. Phys.* **1964**, *41*, 760−764.
(60) Giannozzi, P.; de Gironcoli, S.; Pavone, P.; Baroni, S. Ab Initio Calculation of Phonon Dispersions in Semiconductors. *Phys. Rev. B* **1991**, *43*, 7231−7242.
(61) Gonze, X. First-Principles Responses of Solids to Atomic Displacements and Homogeneous Electric Fields: Implementation of a Conjugate-Gradient Algorithm. *Phys. Rev. B* **1997**, *55*, 10337−10354.
(62) Irikura, K. K. Experimental Vibrational Zero-Point Energies: Diatomic Molecules. *J. Phys. Chem. Ref. Data* **2007**, *36*, 389−397.

https://doi.org/10.1021/acs.jpcc.2c02213
J. Phys. Chem. C 2022, 126, 11358−11364